A Stationary Reference Frame Grid Synchronization System for Three-Phase Grid-Connected Power Converters Under Adverse Grid Conditions

Pedro Rodríguez, *Senior Member, IEEE*, Alvaro Luna, *Member, IEEE*, Raúl Santiago Muñoz-Aguilar, Ion Etxeberria-Otadui, *Member, IEEE*, Remus Teodorescu, *Senior Member, IEEE*, and Frede Blaabjerg, *Fellow, IEEE*

***Abstract*—Grid synchronization algorithms are of great importance in the control of grid-connected power converters, as fast and accurate detection of the grid voltage parameters is crucial in order to implement stable control strategies under generic grid conditions. This paper presents a new grid synchronization method for three-phase three-wire networks, namely dual second-order generalized integrator (SOGI) frequency-locked loop. The method is based on two adaptive filters, implemented by using a SOGI on the stationary $\alpha\beta$ reference frame, and it is able to perform an excellent estimation of the instantaneous symmetrical components of the grid voltage under unbalanced and distorted grid conditions. This paper analyzes the performance of the proposed synchronization method including different design issues. Moreover, the behavior of the method for synchronizing with highly unbalanced grid is proven by means of simulation and experimental results, demonstrating its excellent performance.**

***Index Terms*—Adaptive filters (AFs), electric variables measurements, frequency-locked loops (FLLs), monitoring, power converters, renewables, smart grid, synchronization.**

I. Introduction

NOWADAYS, the use of power electronics and information and communication technology (ICT) applications are key issues in the development of future electrical networks. The high penetration of renewable energy sources [1], such as wind power and photovoltaics [2], experienced in the last decades is a good example, as both generation systems are connected to the grid by means of power electronics-based power processors [3], that should not only control the power delivered to the network, but also contribute to the grid stability, supporting the grid services (voltage/frequency) under generic conditions, even under grid faults [4]–[8].

One of the most important issues in the connection of power converters to the grid is the synchronization with the grid voltage at the point of common coupling (PCC) [9], [10]. Although the grid voltage waveforms are sinusoidal and balanced under regular operating conditions, they can easily become unbalanced and distorted due to the effect of grid faults and nonlinear loads. Under these conditions, grid-connected converters should be properly synchronized with the grid in order to stay actively connected, supporting the grid services and keeping the generation up and running [11]–[15]. Actually, these are currently former requirements in all grid codes (GCs) for the connection of distributed generation systems to the network, where the criteria for the injection of active and reactive power during either balanced or unbalanced grid fault conditions are also provided. Despite the fact that the dynamics of grid synchronization are not established in the GC, requirements are needed in order to achieve a certain dynamical response in the synchronization [16].

Algorithms based on the implementation of phase-locked loops (PLL) have traditionally been used for synchronizing the control system of power converters with the grid voltage. In Fig. 1, the layout of a generic control structure for a three-phase power converter connected to the grid is shown. As depicted in Fig. 1, the grid synchronization block is responsible for estimating the magnitude frequency and phase angle of the positive- and the negative-sequence components of the grid voltage, $\mathbf{v}^{\pm}$, ω, and $\theta^{\pm}$, respectively. These estimated values are later used at the current controller block, which settles finally the voltage waveform to be modulated $\mathbf{v}_c^*$ as well as at the reference

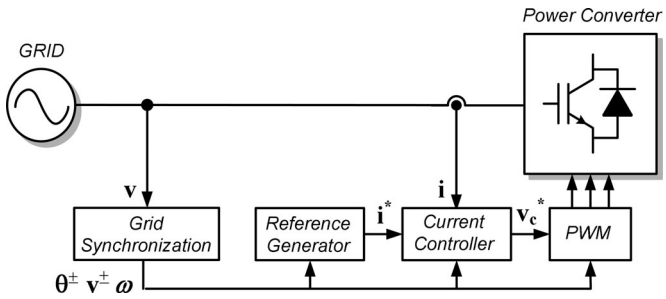

Fig. 1. Generic grid synchronization application for the control of a grid-connected three-phase power converter.

Manuscript received November 6, 2010; revised February 24, 2011; accepted March 11, 2011. Date of current version December 16, 2011. This work was supported by the Spanish Ministry of Science and Innovation under the Project ENE2008-06841-C02-01/ALT and Project TRA2009-0103. Recommended for publication by Associate Editor B. Wu.

P. Rodriguez, A. Luna, and R. Muñoz-Aguilar are with the Department of Electrical Engineering, Technical University of Catalonia, 08222 Terrassa-Barcelona, Spain (e-mail: prodriguez@ee.upc.edu; luna@ee.upc.edu; raul.munoz-aguilar@upc.edu).

I. Etxeberria-Otadui is with the IKERLAN-IK4 Technological Research Center, 20500 Arrasate-Mondragon, Spain (e-mail: ietxeberria@ikerlan.es).

R. Teodorescu and F. Blaabjerg are with the Department of Energy Technology, Aalborg University, 9220 Aalborg East, Denmark (e-mail: ret@iet.aau.dk; fbl@et.aau.dk).

Color versions of one or more of the figures in this paper are available online at http://ieeexplore.ieee.org.

Digital Object Identifier 10.1109/TPEL.2011.2159242

generator, responsible of determining the current reference to be tracked. This last block will vary if the power converter is acting as an active filter, a STATCOM, or a power processor belonging to a power generation plant.

In three-phase systems, a PLL based on a synchronous reference frame (SRF-PLL) [17] has become a conventional grid synchronization technique. Nevertheless, the response of the SRF-PLL is unacceptably deficient when the grid voltage is unbalanced due to the appearance of a negative-sequence component that the SRF-PLL is unable to process properly. In order to solve this problem, different advanced grid synchronization systems have recently been proposed.

This is the case of the decoupled double SRF PLL (DDSRF-PLL) [18], an extension of the SRF-PLL, which uses two SRFs and a decoupling network to isolate the effects of the positive- and the negative-sequence voltage components. Another interesting synchronization technique was presented in [19], where three single-phase enhanced PLLs are combined with a positive-sequence calculator to synchronize with unbalanced and distorted three-phase networks without using any SRF.

Considering the same structure, other single-phase PLL approaches, like those presented in [20]–[23], can be used to provide the input signals to the positive-sequence calculation algorithm. Likewise, other synchronization structures have been proposed for three-phase systems based on PLL, as those published in [24]–[26]. However, the dynamical response of these algorithms is very sensitive to phase angle jumps in the voltage at the PCC due the fact that the PLL is synchronizing with this variable. This is a serious drawback, as sudden phase angle changes are prone to happen when a fault occurs, due to the change in the network impedance.

In this paper, a new approach using frequency locking instead of conventional phase locking will be presented as an effective solution for grid synchronization under adverse grid conditions. The proposed synchronization system is based on the basic operation principle presented in [27] and [28], on an adaptive filter (AF), implemented by means of a second-order generalized integrator (SOGI), which is self-tuned to the grid frequency thanks to the action of a frequency-locked loop (FLL). Therefore, the proposed synchronization system has been called SOGI-FLL.

First, special attention is paid to the description of the main building blocks of the synchronization system, the SOGI and the FLL. The single-phase SOGI-FLL is analyzed in deep, where the FLL performance is linearized and the tuning of the system parameters is discussed. The application of the SOGI-FLL to three-phase three-wire systems is presented, giving rise to a new structure called dual SOGI-FLL (DSOGI-FLL). Finally, the method is simulated and tested under different conditions. Considering that the applications of power converters may be diverse, the application used for illustrating the performance of the synchronization system in this paper has been mainly focused in those where the power converter is responsible for delivering power into the network, as part of a distributed generation power plant, as well as in those related to applications devoted to improving grid stability.

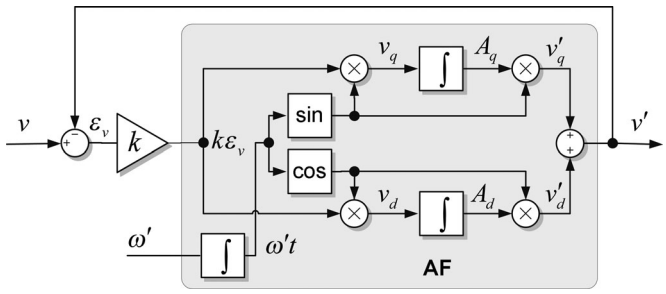

Fig. 2. Single-frequency adaptive noise canceller.

II. AF With an FLL (SOGI-FLL)

The synchronization system proposed in this paper is based on an AF whose tuning frequency is set by an FLL. The operating principle of the SOGI-FLL proposed in this paper is similar to the adaptive noise canceling technique [29], [30]. A modified version in the continuous time domain of the single-frequency adaptive noise canceller in [29] is shown in Fig. 2. In this case, it can be noticed how the auxiliary signal ω' is responsible for setting the frequency of the sinusoidal interference to be canceled from the primary input signal v. These sinusoidal signals are internally generated by the sine and cosine blocks. Considering v' and $k\varepsilon_v$ as the output and input signals, respectively, the transfer function of the AF in Fig. 2 is given by

$$\mathrm{AF}(s) = \frac{v'}{k\varepsilon_v}(s) = \frac{s}{s^2 + \omega'^2} \tag{1}$$

where ω' is the frequency value of the signals to be canceled in rad/s and k is the gain of the canceller.

From (1), it can be seen that the AF in Fig. 2 acts as a sinusoidal integrator at the frequency ω'. In fact, the transfer function shown in (1) matches a generalized integrator (GI) for sinusoidal signals [31]. The GI is a mathematical concept that originates from the principle that the time-domain convolution product of a sinusoidal function by itself gives rise to a sinusoidal term multiplied by the time variable [31]. As a consequence, a processing block whose transfer function is equal to a sinusoidal function of the frequency ω', which is the case of (1), will act as an "amplitude integrator" for any sinusoid with the same frequency applied to its input.

The GI is the base of proportional-resonant controllers [32]–[35], and it can be applied both to AF and PLL implementations [36]. Fig. 3(a) shows the filtering structure described in [36].

It is worth pointing out that the transfer function of the GI implemented in [36] matches perfectly the transfer function of the AF shown in (1), i.e., AF(s) = GI(s). Hence, the filtering structures in Figs. 2 and 3(a) are equivalent and both will exhibit the same dynamic performance when acting as adaptive noise cancellers.

A. AF Based on an SOGI

An interesting feature of the GI, when it is used in power converter synchronization applications, is its ability to generate a set of in-quadrature output signals. In the control of grid-connected power converters, these in-quadrature signals are used to

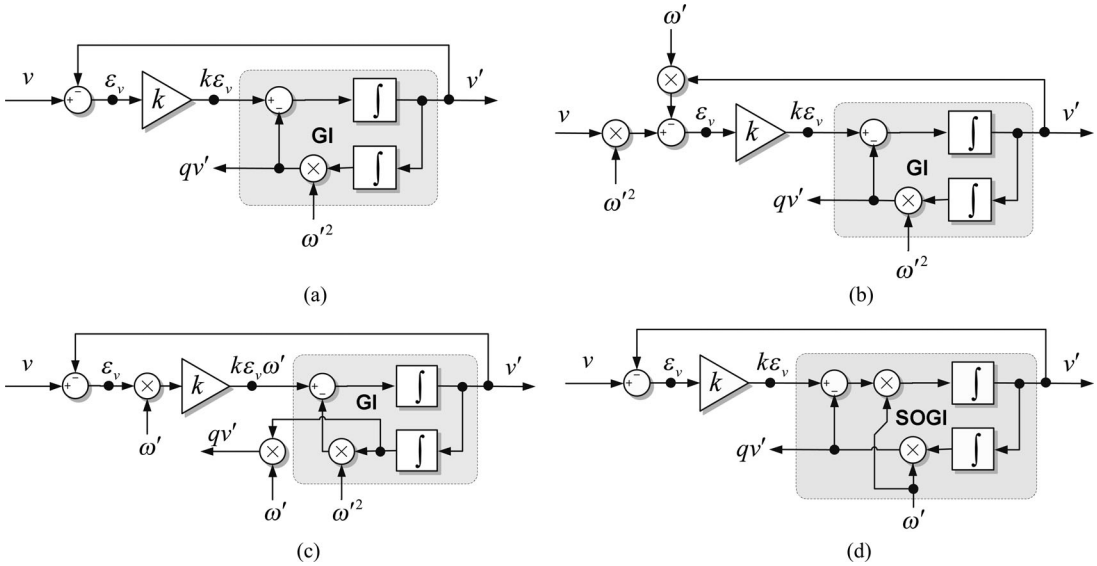

Fig. 3. Different structures of AFs based on GIs. (a) GI Structure. (b) GI with a bandwidth independent of the frequency ω'. (c) GI with a bandwidth independent of the frequency ω' and normalized output amplitude. (d) SOGI structure.

estimate the rms value of the grid voltage and current, to calculate the active and reactive power references for the power converter, to generate a leaded/lagged version of the power signal, and to compute the positive- and negative-sequence components in three-phase systems. The two in-quadrature output signals of the AF in Fig. 3(a) are given by the following transfer functions

$$D(s) = \frac{v'}{v}(s) = \frac{ks}{s^2 + ks + \omega'^2} \tag{2a}$$

$$Q(s) = \frac{qv'}{v}(s) = \frac{k\omega'^2}{s^2 + ks + \omega'^2} \tag{2b}$$

where ω' and k are the tuning frequency and the damping factor of the filter, respectively, while v' and qv' are the in-phase and in-quadrature signals of the input v. Even though the v' and qv' signals are in-quadrature, the transfer functions of (2a) and (2b) are not the most suitable choices for implementing a frequency-variable AF, as the bandwidth of (2a) and the steady-state gain of (2b) are not only a function of the gain k, but also depend on the center frequency of the filter ω' which indeed is the resonance frequency of the GI.

A solution to overcome this problem was addressed in [37], where the input signal v was scaled by ω'^2 and the feedback signal v' was multiplied by ω', as shown in Fig. 3(b). As a result, the two in-quadrature output signals of the AF in Fig. 3(b) are given by,

$$D(s) = \frac{v'}{v}(s) = \frac{k\omega'^2 s}{s^2 + k\omega' s + \omega'^2} \tag{3a}$$

$$Q(s) = \frac{qv'}{v}(s) = \frac{k\omega'^4}{s^2 + k\omega' s + \omega'^2}. \tag{3b}$$

The bandwidths of (3a) and (3b) are independent of the center frequency ω', being exclusively set by the gain k. However, the amplitudes of both components do not match the amplitudes of the input signals when the centre frequency ω' is equal to the input frequency ω.

An alternative to the AF in Fig. 3(a) is shown in Fig. 3(c) [38]. In this case, the in-quadrature transfer functions are given by

$$D(s) = \frac{v'}{v}(s) = \frac{k\omega' s}{s^2 + k\omega' s + \omega'^2} \tag{4a}$$

$$Q(s) = \frac{qv'}{v}(s) = \frac{k\omega'^2}{s^2 + k\omega' s + \omega'^2}. \tag{4b}$$

The AF in Fig. 3(c) can be considered as a proper solution to synchronize grid-connected power converters, since the bandwidth of the AF depends only on the gain k, and the amplitude of the in-quadrature signals v' and qv' matches the amplitude of the signal v when the input frequency ω is equal to the center frequency of the filter ω'.

Finally, instead of modifying the structure of the AF, an alternative structure for the GI is proposed in order to achieve the transfer functions written in (4). The new sinusoidal integrator, which is shown in Fig. 3(d), is called the SOGI [39], [40]. The SOGI transfer function is given by

$$\mathrm{SOGI}(s) = \frac{v'}{k\varepsilon_v}(s) = \frac{\omega' s}{s^2 + \omega'^2}. \tag{5}$$

The AFs shown in Fig. 3(c) and (d) are equivalent and have the same dynamic response. However, the AF based on the SOGI is simpler than the one shown in Fig. 3(c), since the detected frequency ω' does not have to be squared and one less multiplication is necessary.

B. FLL

The center frequency of the structures in Fig. 3(c) and (d) should be adapted to the frequency of the input signal in order to achieve a balanced set of in-quadrature outputs with the correct amplitudes. In fact, the frequency adaptation mechanisms for these structures share a common philosophy. The FLL for the

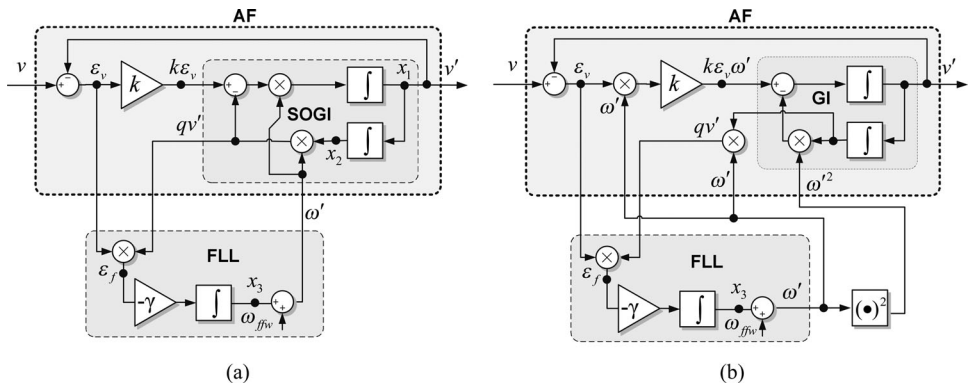

Fig. 4. Single-phase grid-synchronization system. (a) SOGI-FLL. (b) ANF based with an FLL.

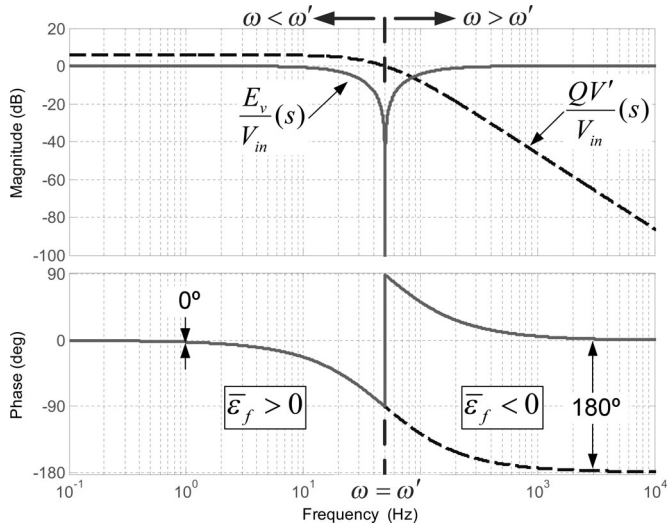

Fig. 5. *Bode* diagram of the FLL input variables.

AF based on the SOGI in Fig. 3(d), which was presented in [35], is shown in Fig. 4(a).

Considering that the transfer function from the input signal v to the error signal ε_v is given by $E(s)$, as written in (6), and plotting both $E(s)$ and $Q(s)$ together in the *Bode* diagram shown in Fig. 5, it can be seen that the signals qv' and ε_v are in phase when the input frequency is lower than the SOGI resonance frequency $\omega<\omega'$ and they are in counterphase when $\omega> \omega'$

$$E(s) = \frac{\varepsilon_v}{v}(s) = \frac{s^2 + \omega'^2}{s^2 + k\omega' s + \omega'^2}. \tag{6}$$

If a frequency error variable ε_f is defined as the product of qv' by ε_v, the average value of ε_f will be positive when $\omega < \omega'$, zero when $\omega = \omega'$, and negative when $\omega > \omega'$, as is shown in Fig. 5. Hence, as illustrated in Fig. 4(a), an integral controller with a negative gain $-\gamma$ can be used to cancel the dc component of ε_f by shifting the SOGI resonance frequency ω' until matching the input frequency ω. As shown in Fig. 4(a), the nominal value of the grid frequency can be added to the FLL output as a feedforward variable ω_{ffw} to accelerate the initial synchronization process. The frequency adaptation mechanism of the SOGI structure in Fig. 3(d), an adaptive notch filter (ANF), is shown in Fig. 4(b). Since the transfer functions of the SOGI-FLL and the ANF are identical, it seems reasonable that both filters share the same FLL mechanism. However, as shown in Fig. 4, the interconnection between the FLL and the SOGI is simpler in the SOGI-FLL than in the ANF.

The combination of the SOGI and the FLL building blocks, as shown in Fig. 4(a), gives rise to a single-phase grid synchronization system known as SOGI-FLL. In the SOGI-FLL, the input frequency is directly detected by the FLL, while the estimation of the phase angle and the amplitude of the input "virtual vector" $\mathbf{v}'$ can be indirectly calculated as written in

$$|\mathbf{v}'| = \sqrt{(v')^2 + (qv')^2}\ ; \qquad \underline{|\mathbf{v}'} = \arctan\frac{qv'}{v'} \tag{7}$$

where v' and qv' are the in-phase and in-quadrature signals of the input signal v. The performance and dynamical response of the SOGI-FLL depend mainly on the appropriate selection of the control parameters k and γ.

III. Tuning of the SOGI-FLL

The space-state equations of the SOGI-FLL, written in (8 (a)–(c)), can be obtained from the diagram shown in Fig. 4(a), where **x** in (8a) is the state vector of the SOGI and **y** in (8b) is the output vector, while the state equation describing the behavior of the FLL is shown in (8c)

$$\dot{\mathbf{x}} = \begin{bmatrix} \dot{x}_1 \\ \dot{x}_2 \end{bmatrix} = \mathbf{A}\mathbf{x} + \mathbf{B}v = \begin{bmatrix} -k\omega' & -\omega'^2 \\ 1 & 0 \end{bmatrix} \begin{bmatrix} x_1 \\ x_2 \end{bmatrix} + \begin{bmatrix} k\omega' \\ 0 \end{bmatrix} v \tag{8a}$$

$$\mathbf{y} = \begin{bmatrix} v' \\ qv' \end{bmatrix} = \mathbf{C}\mathbf{x} = \begin{bmatrix} 1 & 0 \\ 0 & \omega' \end{bmatrix} \begin{bmatrix} x_1 \\ x_2 \end{bmatrix} \tag{8b}$$

$$\dot{\omega}' = -\gamma x_2 \omega' (v - x_1). \tag{8c}$$

Considering the stable operating conditions that implies $\dot{\omega}' = 0$ and $\omega = \omega'$, (8a) can be written as shown in (9), in which the

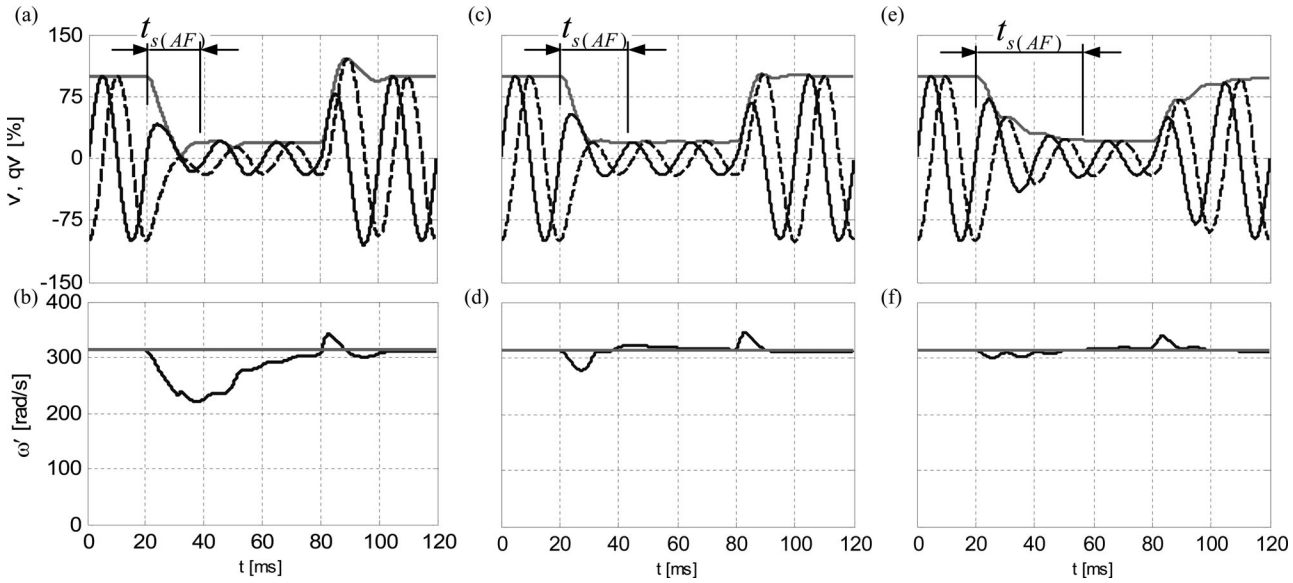

Fig. 6. Time response of the SOGI when an 80% voltage drop occurs. (a) Positive-sequence magnitude estimation and v' and qv' signals. (b) Frequency estimation with $k = 2.5$. (c) Positive-sequence magnitude estimation and v' and qv' signals. (d) Frequency estimation with $k = \sqrt{2}$. (e) Positive-sequence magnitude estimation and v' and qv' signals. (f) Frequency estimation with $k = 0.6$.

steady-state variables are indicated with a bar over.

$$\dot{\bar{\mathbf{x}}}_{|\dot{\omega}'=0} = \begin{bmatrix} \dot{\bar{x}}_1 \\ \dot{\bar{x}}_2 \end{bmatrix} = \begin{bmatrix} 0 & -\omega'^2 \\ 1 & 0 \end{bmatrix} \begin{bmatrix} \bar{x}_1 \\ \bar{x}_2 \end{bmatrix}. \tag{9}$$

The eigenvalues of the Jacobian that can be obtained from (9) have a null real part, something that confirms the resonant behavior of the system, as the steady-state response remains in a periodic orbit at the ω' frequency [41]. Therefore, for a given sinusoidal input signal $v = V \sin(\omega t + \phi)$, the steady-state output vector will be given by

$$\bar{\mathbf{y}} = \begin{bmatrix} v' \\ qv' \end{bmatrix} = V \begin{bmatrix} \sin(\omega t + \phi) \\ -\cos(\omega t + \phi) \end{bmatrix}. \tag{10}$$

If the FLL was intentionally frozen at a frequency different from the input-signal frequency $\omega \neq \omega'$, e.g., by making $\gamma = 0$, the output vector would still keep in a stable orbit defined by

$$\bar{\mathbf{y}}' = V\,|D(j\omega)| \begin{bmatrix} \sin(\omega t + \phi + \angle D(j\omega)) \\ -\dfrac{\omega'}{\omega} \cos(\omega t + \phi + \angle D(j\omega)) \end{bmatrix} \tag{11}$$

where $|D(j\omega)|$ and $\angle D(j\omega)$ can be written as shown in

$$|D(j\omega)| = \frac{k\omega\omega'}{\sqrt{(k\omega\omega')^2 + (\omega^2 - \omega'^2)^2}},$$
$$\angle D(j\omega) = \arctan \frac{\omega'^2 - \omega^2}{k\omega\omega'}. \tag{12}$$

A. SOGI Tuning

From the transfer functions of (4), and considering the input frequency ω as a constant, the time response of the SOGI in Fig. 4(a) for a given sinusoidal input signal $v = V \sin(\omega t + \phi)$ is written as

$$v' = -\frac{V}{\lambda} \sin(\lambda\omega t) \cdot e^{-(k\omega'/2)t} + V \sin(\omega t) \tag{13a}$$

$$qv' = V \left[\cos(\lambda\omega t) + \frac{k}{2\lambda} \cdot \sin(\lambda\omega t) \right] e^{-(k\omega'/2)t} - V \cos(\omega t) \tag{13b}$$

where $\lambda = \sqrt{4 - k^2}/2$ and $k < 2$.

According to (13(a), (b)), the settling time in the SOGI response can be approximated to

$$t_{s(\mathrm{AF})} = \frac{10}{k\omega'}. \tag{14}$$

As it can be concluded from (14), the higher the value of k, the faster the response of the SOGI. However, the gain k affects also the bandwidth of the SOGI, a very high value for k would reduce the immunity of the SOGI in front of harmonics in the input, but, on the other hand, a very low value for k gives rise to a very long undamped transient response of the SOGI. Fig. 6 shows the response of the SOGI considering different values of k. In all cases, the amplitude of the sinusoidal input signal drops down to 20% of its rated value while its frequency keeps constant at 50 Hz. In Fig. 6(a) and (b), the estimation of the positive-sequence voltage and the grid frequency is shown when $k = 2.5$. In Fig. 6(c) and (d), the response of the SOGI-FLL is presented when $k = \sqrt{2}$. Finally, Fig. 6(e) and (f) shows the behavior of the positive sequence and the frequency estimation, respectively, when k is reduced to 0.6.

As it can be concluded from Fig. 6(c) and (d), the better tradeoff between dynamical response and overshooting can be achieved with $k = \sqrt{2}$. Moreover, even though the frequency detected by the FLL shows some transient oscillations when the

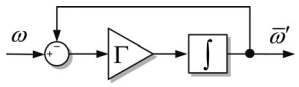

Fig. 7. Simplified frequency adaptation system of the FLL.

input-voltage level varies, the settle time in response of the SOGI matches the 22.5 ms obtained from (14).

B. FLL Tuning

Linear control analysis techniques cannot directly be applied to determine the value of the FLL gain γ, since the frequency-adaptation loop is highly nonlinear. Hence, some assumptions should be made to determine the performance of the FLL.

Considering a sinusoidal signal $v = V\sin(\omega t + \phi)$ as the input signal for the SOGI and assuming nonstable FLL operating point, with $\omega' \neq \omega$, the square of the state $\bar{x}_2$ can be written from (11) as

$$\bar{x}_2^2 = \frac{V^2}{2\omega^2}\left|D(j\omega)\right|^2\left[1+\cos\left(2\left(\omega t+\phi+\angle D(j\omega)\right)\right)\right]. \quad (15)$$

The terms $|D(j\omega)|$ and $\angle D(j\omega)$ in (15) tend toward 1 and 0, respectively, as the frequency detected by the FLL locks the input frequency $\omega' \to \omega$. Hence, in the vicinity of the steady-state operation of the FLL, $\bar{x}_2^2$ will present a dc component equal to $V^2/2\omega^2$ plus an ac term oscillating at twice the input frequency. As was shown in [43], the averaged dynamics of the FLL with $\omega' \approx \omega$ can be described by (16), where the ac component of $\bar{x}_2^2$ has been neglected

$$\dot{\bar{\omega}}' = -\frac{\gamma V^2}{k\omega'}\left(\bar{\omega}' - \omega\right). \quad (16)$$

The state equation of (16) is very interesting because it discloses the relationship between the dynamic response of the FLL, the grid variables, and the SOGI gain. From (16), the value of γ can be normalized according to

$$\gamma = \frac{k\omega'}{V^2}\Gamma \quad (17)$$

where V is the magnitude of the input voltage, k is the gain of the SOGI, ω' is the estimated frequency, and Γ is the parameter that permits regulating the settling time of the grid-synchronization loop. The linear control loop that can be built by means of (16) and (17) is graphically presented in Fig. 7.

The transfer function of the first-order frequency-adaptation loop in Fig. 7 is given by

$$\frac{\bar{\omega}'}{\omega} = \frac{\Gamma}{s+\Gamma}. \quad (18)$$

Therefore, the settling time is exclusively dependent on the design parameter Γ and can be approximated by [42]

$$t_{s(\mathrm{FLL})} \approx \frac{5}{\Gamma}. \quad (19)$$

A practical implementation of the feedback-based linearized FLL is shown in Fig. 8.

In this system, the FLL gain is online adjusted by feeding back the estimated grid-operating conditions, which guarantees a constant settle time in the grid-frequency estimation independently of the input signal characteristics.

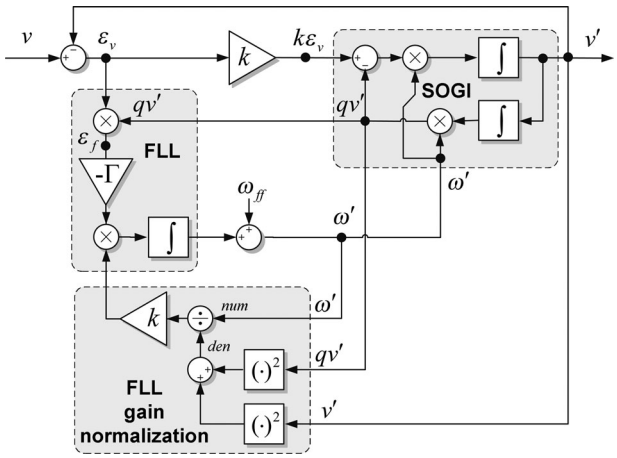

Fig. 8. SOGI-FLL with FLL-gain normalization.

It is worth noting that the output of the FLL-gain normalization block in Fig. 8 has been limited to a maximum value in that case in which the grid voltage drops to zero.

Fig. 9 shows the time response of an SOGI-FLL with $k = \sqrt{2}$ and different values of Γ when the frequency of the input signal suddenly varies from 50 to 60 Hz. In Fig. 9(a), the estimation of the positive-sequence magnitude and the v' and qv' signals are shown, while in Fig. 9(b) the estimation of the frequency performed by the FLL, as well as its approximated first-order response, is shown when $\Gamma = 100$.

As shown in Fig. 9(b), this value of Γ gives rise to a settling time of $t_{s(\mathrm{FLL})} = 50$ ms according to (19).

Analogous results can be found in Fig. 9(c) and (d) where the same variables are shown when using $\Gamma = 50$, reaching a settling time of $t_{s(\mathrm{FLL})} = 100$ ms. Likewise, a slower dynamic response is reported also in Fig. 9(e) and (f) when using $\Gamma = 33.3$. From the results shown in Fig. 9, it can be stated that, in all cases, the detected frequency fits well a first-order exponential response matching to that calculated by (19).

At this point, it is worth mentioning that the SOGI and the FLL have been studied by considering separated variations in both the amplitude and the frequency of the input signal. However, both systems are independent, which means that the global time response of the SOGI-FLL will differ from the one obtained whether the input signal experiments simultaneous variations in frequency and amplitude. However, from an analysis based on simulation, it could be considered that the settling times of SOGI and FLL will continue matching to those calculated by (14) and (19) if the settle times are in the range of $t_{S(\mathrm{FLL})} \geq 2 \cdot t_{S(\mathrm{SOGI})}$ for $k = \sqrt{2}$, where $t_{s(\mathrm{FLL})}$ and $t_{s(\mathrm{SOGI})}$ are the settling times of the FLL and the SOGI, respectively, while k is the SOGI gain. From now on, a value of $k = \sqrt{2}$ and $\Gamma = 50$ will be considered for the following simulations and experiments.

As has been demonstrated with these parameters, the frequency is estimated by the FLL with no error after 100 ms, while the error is within 5% just after 20 ms. This response is even faster for the SOGI. This dynamical response would permit

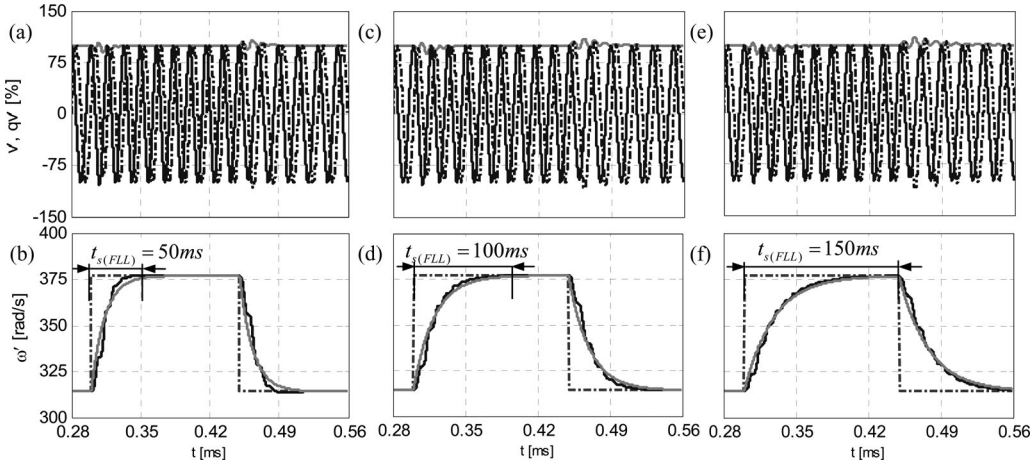

Fig. 9. Time response of the FLL in the presence of a frequency step (from 50 to 60 Hz). (a) Positive-sequence magnitude estimation and v' and qv' signals. (b) Frequency estimation with $\Gamma = 100$ ($t_{s\,(\mathrm{FLL})} = 50$ ms). (c) Positive-sequence magnitude estimation and v' and qv' signals. (d) Frequency estimation with $\Gamma = 50$ ($t_{s\,(\mathrm{FLL})} = 100$ ms). (e) Positive-sequence magnitude estimation and v' and qv' signals. (f) Frequency estimation with $\Gamma = 33.3$ ($t_{s\,(\mathrm{FLL})} = 150$ ms).

us to fulfill the implicit time response required by the Spanish and German GCs, regarding the injection of reactive currents 20 ms after the detection of a grid fault.

Although a faster response could be achieved, both $k = \sqrt{2}$ and $\Gamma = 50$ offer a good tradeoff between the bandwidth of the SOGI-FLL and its sensitivity in front of harmonics and noisy signals affecting the synchronization system.

IV. SOGI-FLL Applied to Three-Phase Systems

Nowadays, a high proportion of the three-phase power converters are connected to three-phase three-wire networks. In this section, an extension of the SOGI-FLL single-phase algorithm will be proposed for three-phase applications. This synchronization algorithm allows estimating of the instantaneous symmetrical components of the grid voltage in the $\alpha\beta$ domain, as well as the frequency value, with no need of using any SRF.

A. Instantaneous Symmetrical Components

According to Lyon's method [44], a voltage vector $\mathbf{v}_{\mathrm{abc}}$ consisting of three unbalanced sinusoidal waveforms can be split into its instantaneous positive-, negative-, and zero-sequence components $\mathbf{v}_{abc} = \mathbf{v}^{+}_{abc} + \mathbf{v}^{-}_{abc} + \mathbf{v}^{0}_{abc}$. These components can be found through Lyon's tranformations $[T_+]$, $[T_-]$, and $[T_0]$.

Most of the three-phase grid-connected power converters employ a three-wire connection. Therefore, the current injected into the network is exclusively synchronized with the positive- and negative-sequence components of the grid voltage. As a direct consequence, the three-phase voltage vector can be represented in an orthogonal reference frame by means of two independent variables $\alpha\beta$ thanks to the *Clarke* transformation. Moreover, taking advantage of Lyon's transformations, the instantaneous positive- and negative-sequence voltage components on the $\alpha\beta$ reference frame can be calculated as written in

$$\begin{aligned}\mathbf{v}^{+}_{\alpha\beta} &= [T_{\alpha\beta}]\ \mathbf{v}^{+}_{abc} = [T_{\alpha\beta}]\,[T_+]\,\mathbf{v}_{abc} \\ &= [T_{\alpha\beta}]\,[T_+]\,[T_{\alpha\beta}]^T\,\mathbf{v}_{\alpha\beta} = \frac{1}{2}\begin{bmatrix}1 & -q\\ q & 1\end{bmatrix}\mathbf{v}_{\alpha\beta} \quad (20)\end{aligned}$$

$$\begin{aligned}\mathbf{v}^{-}_{\alpha\beta} &= [T_{\alpha\beta}]\ \mathbf{v}^{-}_{abc} = [T_{\alpha\beta}]\,[T_-]\,\mathbf{v}_{abc} \\ &= [T_{\alpha\beta}]\,[T_-]\,[T_{\alpha\beta}]^T\,\mathbf{v}_{\alpha\beta} = \frac{1}{2}\begin{bmatrix}1 & q\\ -q & 1\end{bmatrix}\mathbf{v}_{\alpha\beta} \quad (21)\end{aligned}$$

where $q = e^{-j(\pi/2)}$ is a 90° lagging phase-shifting operator applied in the time domain to obtain an in-quadrature version of the input waveforms.

B. DSOGI-FLL Structure

Working in the $\alpha\beta$ domain, an optimal application of the SOGI-FLL concept for three-phase grid synchronization applications can be found, giving rise to what is known as the DSOGI-FLL, which is graphically presented in Fig. 10. As can be seen, just two SOGIs are necessary to compute the symmetrical components in a three-phase application, one for α and another for β (AF(α),AF(β). In the DSOGI-FLL in Fig. 10, the two SOGIs are arranged in parallel to provide the input signals to a positive/negative-sequence calculation block (PNSC), which implements the transformations indicated in (20).

Considering that the $\alpha\beta$ components of a balanced positive-sequence voltage vector at frequency ω keep the following steady-state relationship on the frequency domain

$$v_\beta(j\omega) = -jv_\alpha(j\omega) \quad (22)$$

the positive sequence of the voltage vector detected by the DSOGI-FLL, according to (20), can be written as shown in (23), where $D(j\omega)$ and $Q(j\omega)$ are the steady-state transfer functions of the SOGI on the frequency domain as detailed in (4)

$$\begin{aligned}\begin{bmatrix}v^+_\alpha\\ v^+_\beta\end{bmatrix} &= \frac{1}{2}\begin{bmatrix}1 & -q\\ q & 1\end{bmatrix}\begin{bmatrix}v'_\alpha\\ v'_\beta\end{bmatrix} = \frac{1}{2}\begin{bmatrix}D(j\omega) & -Q(j\omega)\\ Q(j\omega) & D(j\omega)\end{bmatrix}\begin{bmatrix}v_\alpha\\ v_\beta\end{bmatrix} \\ &= \frac{1}{2}\left(D(j\omega) + jQ(j\omega)\right)\begin{bmatrix}v_\alpha\\ v_\beta\end{bmatrix} \\ &= \frac{1}{2}\frac{k\omega'\left(\omega+\omega'\right)}{k\omega'\omega + j\left(\omega^2-\omega'^2\right)}\begin{bmatrix}v_\alpha\\ v_\beta\end{bmatrix}. \quad (23)\end{aligned}$$

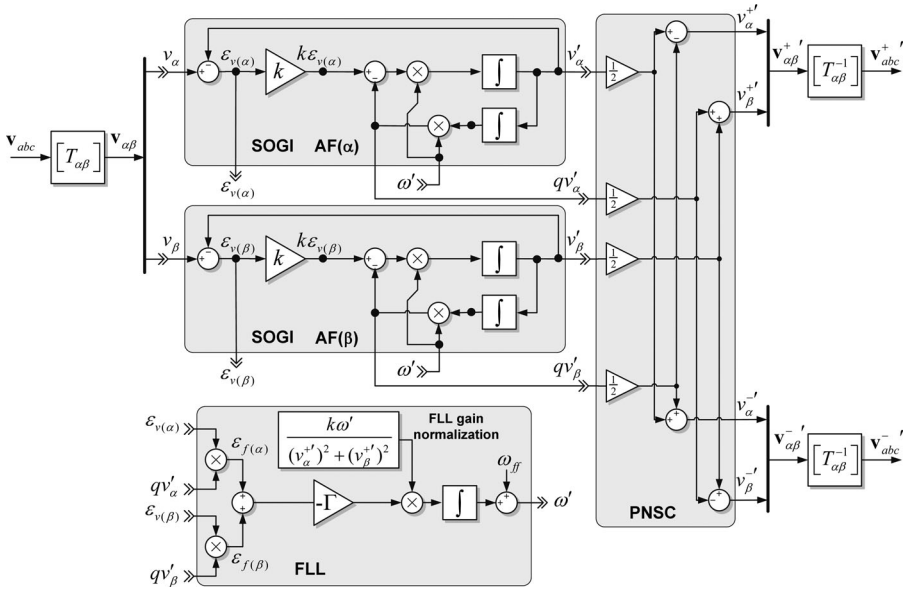

Fig. 10. Block diagram of the DSOGI-FLL.

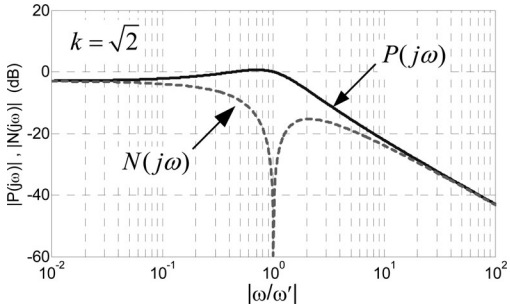

Fig. 11. $P(j\omega)$ is the frequency response of the DSOGI-FLL for the positive-sequence components. $N(j\omega)$ is the response to the negative-sequence components.

The relationship between the amplitude of the positive-sequence component detected by the SOGI-FLL and the actual amplitude of a given positive-sequence voltage vector applied to its input, $P(j\omega) = |\mathbf{v}^{+}_{\alpha\beta}{}'|/|\mathbf{v}^{+}_{\alpha\beta}|$, as well as the relationship between the detected amplitude for the positive-sequence component and the actual amplitude of a given negative-sequence input voltage, $N(j\omega) = |\mathbf{v}^{+}_{\alpha\beta}{}'|/|\mathbf{v}^{-}_{\alpha\beta}|$, is plotted in the *Bode* diagram in Fig. 11

As the *Bode* plot in Fig. 11 shows, the DSOGI-FLL acts either as a low-pass filter or as a notch filter in the detection of the positive-sequence component depending on whether the input voltage shows either positive or negative sequence, respectively.

As stated in Section II, each SOGI of the DSOGI-FLL would have an independent FLL. However, although mathematically correct, the use of two independent FLLs might seem conceptually wrong since the frequency of both v_α and v_β signals are always the same. For this reason, the frequency error signals from both SOGIs of the DSOGI-FLL in Fig. 10 have been combined in a single FLL block. The FLL gain of the system in Fig. 10 is normalized by using the square of the amplitude of the positive-sequence component $(v^{+}_{\alpha})^2 + (v^{+}_{\beta})^2$, which results in a first-order exponential linearized response with the same settling time than the one calculated by (19).

V. Simulation Results

In order to test the response of the DSOGI-FLL, an unbalanced grid voltage sag, affected by jumps in the grid-voltage amplitude, phase angle, and frequency, was applied to its input. In this case, the positive- and the negative-sequence voltage phasors of the grid voltage were $\vec{V}^{+} = 0.5\angle -30^\circ$ (p.u) and $\vec{V}^{-} = 0.25\angle +60^\circ$(p.u) under fault conditions, being the prefault grid voltage equal to $\vec{V}_{\rm pf} = 1\angle 0^\circ$ (p.u). In addition, in the simulated case, the input frequency experienced a sudden jump from 50 to 45 Hz as well when the fault occurred. From Fig. 12(a)–(g), some representative waveforms show the estimation of the symmetrical components performed by the DSOGI-FLL. The tuning parameters of the DSOGI-FLL were set to $k = \sqrt{2}$ and $\Gamma = 50$, as justified in Section III.

In Fig. 12(a), the waveforms of the unbalanced grid voltage are depicted. Fig. 12(b) and (c) shows, respectively, the instantaneous positive- and negative-sequence components detected by the DSOGI-FLL. Likewise, the detected grid-voltage amplitude and phase angle for the symmetrical components are drawn in Fig. 12(d)–(f), respectively. All these values have been calculated according to

$$\left|\mathbf{v}^{\pm\prime}\right| = \sqrt{(v^{\pm}_{\alpha})^2 + \left(v^{\pm}_{\beta}\right)^2}; \qquad \theta^{\pm\prime} = \tan^{-1}\frac{v^{\pm}_{\beta}}{v^{\pm}_{\alpha}}. \tag{24}$$

Finally, the estimation of the grid frequency is shown in Fig. 12(g). As can be noted, the postfault frequency is detected in about 100 ms, matching, hence, the theoretical value that can be calculated through (19). It is worth pointing out from the simulation results shown in Fig. 12(g) that the settling time of the DSOGI-FLL in the frequency estimation almost does not depend on the grid voltage phase-angle jump.

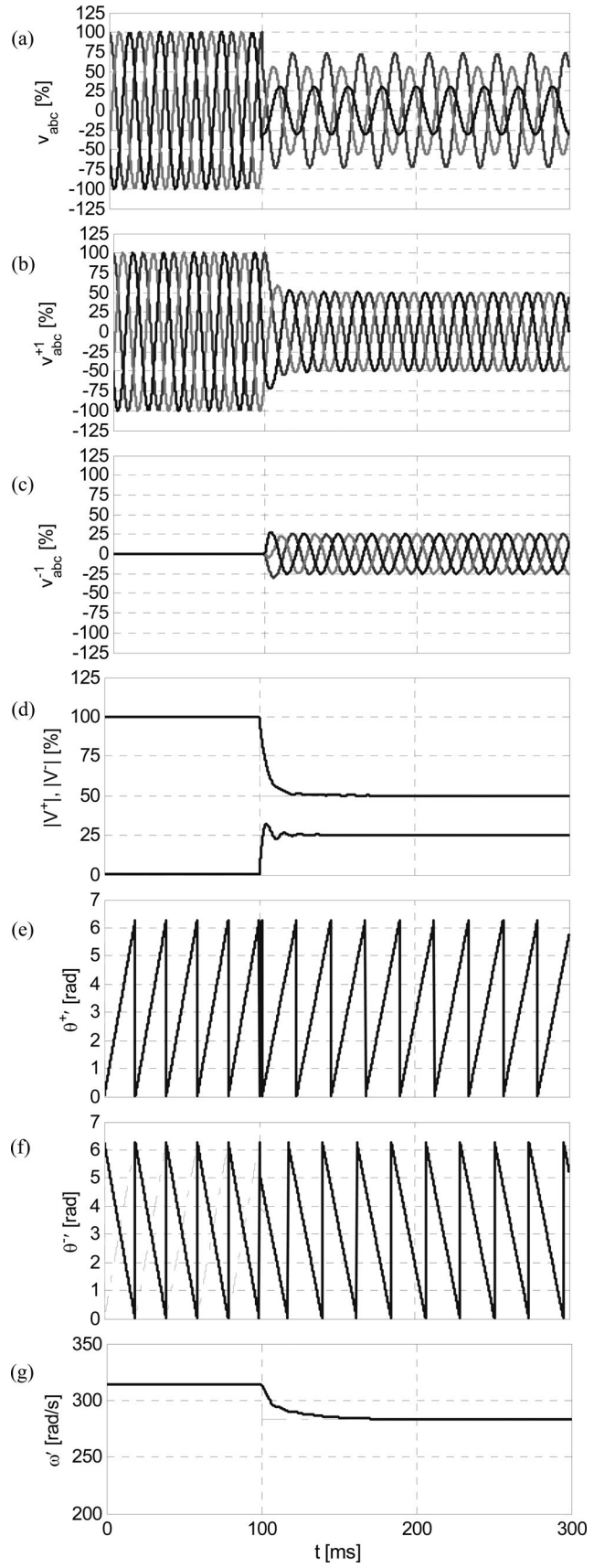

Fig. 12. Response of the DSOGI-FLL with voltage amplitude, phase angle, and frequency changes.

To improve the evaluation of the DSOGI-FLL performance, the voltage sag in Fig. 12(a) was also applied to the input of the SRF-PLL and the DDSRF-PLL. In both cases, the tuning of the control parameters has been set in order to achieve the same time constant of the DSOGI-FLL.

Regarding the SRF-PLL performance, it can be clearly seen in Fig. 13(a)–(d) that this synchronization method is not robust enough under such unbalanced conditions. As shown in Fig. 13(a) and (b), the estimation of the instantaneous positive- and negative-sequence components of the grid voltage is not correct. This is due to the oscillations in both the voltage amplitude and the phase angle estimated by the SRF-PLL under unbalanced conditions as a consequence of the coupling between the positive- and negative-sequence components.

The simulation results depicted in Fig. 13(e)–(h) show the performance of the DDSRF-PLL when the voltage sag in Fig. 12(a) is applied to its input. As is proven in Fig. 13(e) and (f), the positive- and negative-sequence components estimated by the DDSRF-PLL are close to the ones obtained with the DSOGI-FLL. However, as can be noticed in Fig. 13(h), the detection of the grid frequency in the DDSRF-PLL is not as good as the one achieved with the DSOGI-FLL. The DDSRF-PLL is highly influenced by the phase-angle jump of the grid voltage, something that gives rise to a large error in the estimation of such phase angle and, consequently, a large overshoot in the estimated frequency.

From the results presented in this example, it can be concluded that the DSOGI-FLL is a very precise and fast synchronization system which is able to detect without any error the instantaneous positive- and negative-sequence components of the faulty grid voltage in about one grid cycle. This performance cannot be achieved by using a classic SRF-PLL and it is even better than the one achieved with a more advanced grid synchronization system, such as the DDSRF-PLL.

VI. Experimental Results

The DSOGI-FLL was evaluated with an experimental setup in which a faulty grid was emulated by means of a programmable three-phase ac-power source connected to a Δy transformer. The DSOGI-FLL algorithm was implemented in a control board based on a TMS320F28335 DSP that controls a power converter which is connected to the secondary winding of the transformer. The layout of the experimental setup is shown in Fig. 14. The tuning parameters and the sampling period of the DSOGI-FLL were the same as in simulation, i.e., $k = \sqrt{2}$, $\Gamma = 50$,and $T_s = 100\ \mu$s, respectively.

In the first experiment, the capability of the DSOGI-FLL online detecting the positive- and negative-sequence components during a transient grid fault was tested. In this experiment, a single-phase-to-ground fault is generated at the primary winding of the Δy transformer through an impedance $Z_{\rm sc}$ that has been calculated for decreasing the faulty phase from 220 to 110 V rms. The layout of this experiment is described in Fig. 15.

This single-phase-to-ground fault, that constitutes 93–95% of voltage sags in distribution and transmission networks [4], [16], was propagated to the y winding of the figure as a dip type

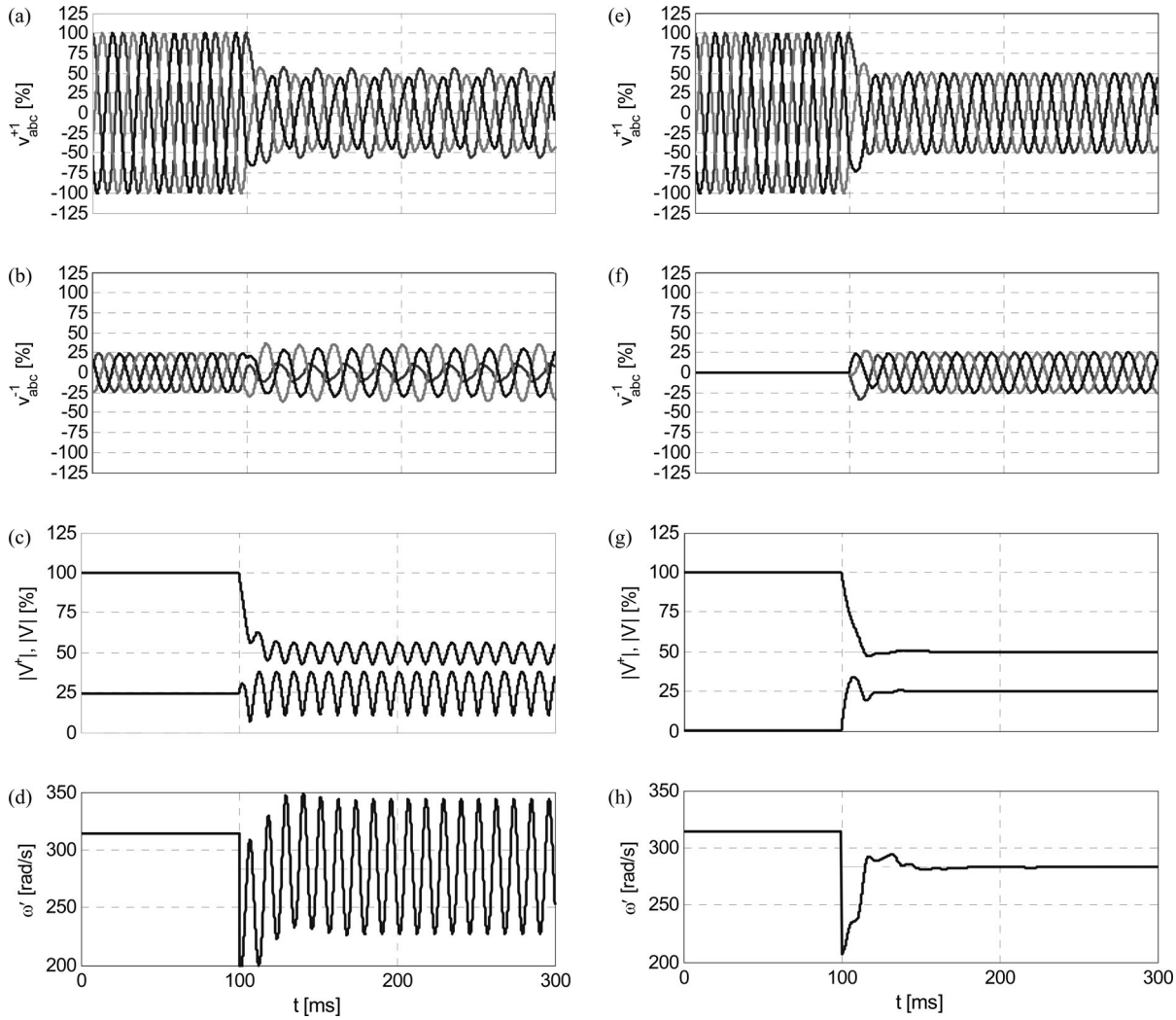

Fig. 13. Transient response of (a)–(d) the SRF-PLL and (e)–(h) the DDSRF-PLL with grid voltage and frequency variations.

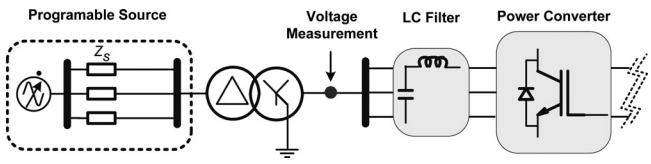

Fig. 14. Layout of the experimental setup.

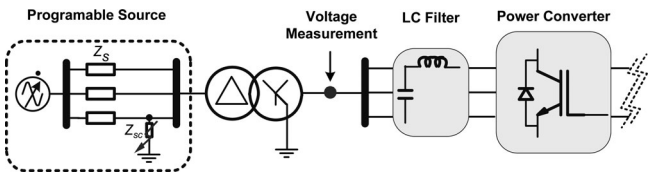

Fig. 15. Generation of a Type C unbalanced voltage sag at the voltage measurement point.

C [45] at the measurement point, with a set of positive- and negative-sequence components given by $\vec{V}^{+} = 0.818\,\underline{|0^\circ}$ p.u. and $\vec{V}^{-} = 0.182\,\underline{|0^\circ}$ p.u., which gave rise to the voltage waveforms depicted in Fig. 16(a). Some plots depicting the online estimation performed by the DSOGI-FLL in this test are shown in Fig. 16(b)–(d), where the magnitude and phase of the estimated positive- and negative-sequence components as well as the instantaneous symmetrical components on the *abc* reference frame have been presented.

As can be noted in Fig. 16(b), the DSOGI-FLL was able to perform a precise estimation of the magnitude and the phase of the symmetrical components in about 50 ms, although after 22.5 ms the fault appearance the error is beyond a narrow 5% margin, as shown in Fig. 16(b). This settling time is equal to the one expected according to (18).

In the second experiment, the capability of the FLL for accurately detecting variations in the grid frequency was tested. In this case, a frequency jump was programed in the ac-power source, giving rise to a sudden step in the grid frequency from 50 to 60 Hz. This 10 Hz jump was selected as a matter of the oscilloscope's resolution that did not permit us to see clearly the performance of the system for lower frequency steps.

In Fig. 17(a), the measured input waveforms are displayed, while the detection of the symmetrical components is shown in Fig. 17(b). In turn, the estimation of the positive sequence

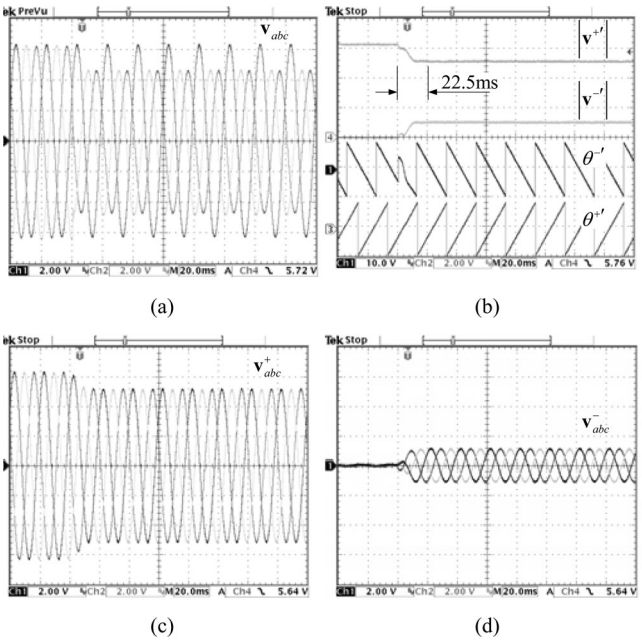

Fig. 16. Experimental evaluation of the DSOGI-FLL in the presence of voltage sags type C. (a) Unbalanced grid voltage. (b) Detected amplitudes and phase angles. (c) Detected positive-sequence signals.(d) Detected negative-sequence signals (Time scale = 20 ms/div).

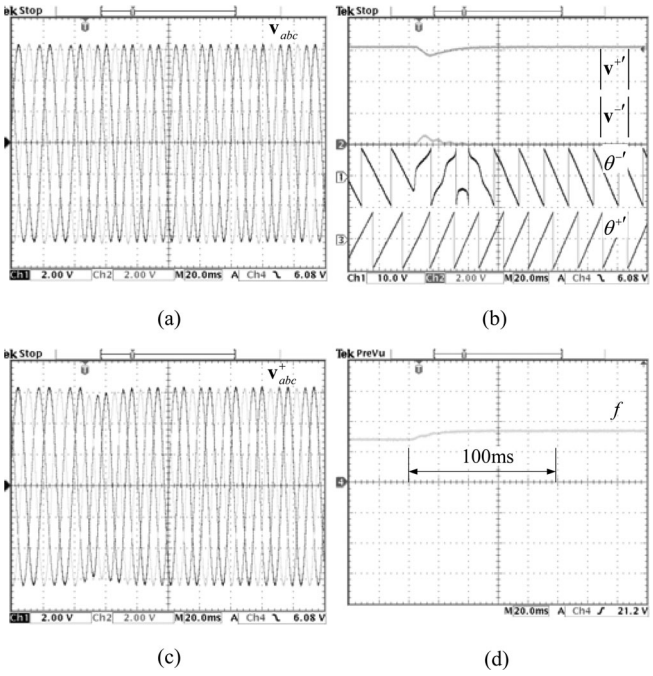

Fig. 17. Experimental evaluation of the DSOGI-FLL in the presence of frequency variation (from 50 to 60 Hz). (a) Unbalanced grid voltage. (b) Detected amplitudes and phase angles. (c) Detected positive-sequence signals. (d) Detected frequency (Time scale = 20 ms/div).

in the *abc* is plotted in Fig. 17(c) where can be noted an expected cross coupling between the frequency and the magnitude detection loops. However, the most interesting information can be extracted from Fig. 17(d), where the detected frequency is shown. Fig. 17(d) validates the frequency-adaptive characteristic of the DSOGI-FLL, which is able to overcome this large jump

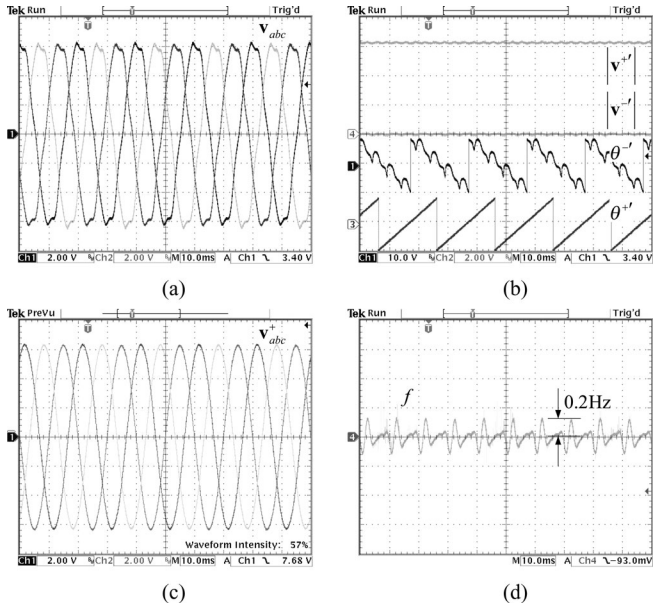

Fig. 18. Experimental evaluation of the DSOGI-FLL in the presence of harmonics (THD = 5%). (a) Harmonic-distorted grid voltage. (b) Amplitudes and phase angles detected. (c) Detected positive-sequence signals. (d) Ripple in the detected frequency (magnified 0.35 Hz/div).

in the grid frequency without oscillations in about 100 ms after following a first-order exponential function, which matches the calculations in (23) and the simulation results in Section V.

Finally, a third experiment was conducted to evaluate the immunity of the DSOGI-FLL in front of distortion in the grid voltage. A distorted waveform with a total harmonic distortion (THD) of 5%, which is shown in Fig. 18(a), was programed in the ac-power source.

In this experiment, it is worth noting the high quality of the detected positive sequence of the voltage, as can be noticed in Fig. 18(b) and (c). Regarding the high level of distortion in the detection of the negative-sequence phase angle $\theta^{-\prime}$, displayed in Fig. 18(b), it can be seen that the negative-sequence component in the measured signal, as fast as the amplitude of the negative-sequence component would rise to higher levels the phase-angle distortion would decrease drastically. It is also necessary to highlight the high precision in the detected frequency under the considered distorted grid conditions, showing a very small ripple of about ± 0.2 Hz over the actual value (50 Hz).

The computational burden time of the DSOGI-FLL has been measured in these tests reaching 5.8 μs in one cycle of instructions of the TMS320F28335 DSP. The result obtained in this test is similar to the ones that can be found with other applications, such as the DSOGI-PLL with 5.91 μs or the DDSRF-PLL with 5.41 μs.

Considering a control step of 100 μs, the burden time of the DSOGI-FLL constitutes no more than 6% of the computational cost of the algorithm; hence, it can be concluded that the DSOGI-FLL can be easily integrated in digital control systems devoted to control power converters without reducing significantly its computational capability.

VII. Conclusion

A new concept in grid synchronization of power converters under unbalanced and faulty operating conditions, the DSOGI-FLL, has been introduced.

The DSOGI-FLL consists of three fundamental blocks: 1) the DSOGI, which uses the SOGI as a building block; 2) an FLL that accurately achieves grid-frequency adaptation without involving phase-angle operations; and 3) the PNSC, which implements the instantaneous symmetrical component (ISC) method on the $\alpha\beta$ reference frame.

The proposed synchronization method exploits the ISC method on the stationary and orthogonal $\alpha\beta$ reference frame, permitting elimination of the zero-sequence component, which cannot be controlled in three-phase three-wire power converters. Moreover, working on the $\alpha\beta$ reference frame permits reduction of the computational cost of the DSOGI-FLL, since no trigonometric transformations should be performed.

As shown in this paper, the presented DSOGI-FLL is a frequency adaptive system that permits synchronizing to the fundamental-frequency component by means of an FLL instead of a PLL. In this paper, it was shown by simulation that voltage phase-angle detection is not a trivial issue under grid fault conditions. Thus, the DSOGI-FLL is less influenced by sudden changes in the voltage phase angle compared with classical or advanced PLLs.

Although a mathematical analysis has demonstrated the nonlinear behavior of the DSOGI-FLL, the application of a feedback-based linearization has permitted us to demonstrate that it is possible to achieve a controllable response of the frequency-adaptation loop as a function of the magnitude and frequency of the input signal. A detailed analysis of the proposed synchronization method has led to expressions that permit setting the tuning parameters in order to achieve a given settle time in the estimation of the amplitude and the frequency of the grid voltage.

The experimental results shown in this paper also demonstrate that the DSOGI-FLL is a very suitable synchronization system for detecting the fundamental-frequency positive- and negative-sequence components of unbalanced three-phase grid voltages.

It can be concluded that the DSOGI-FLL is a very suitable solution when resonant controllers are used to regulate the currents injected into the grid by a power converter. In three-phase three-wire systems, both the tuning frequency and the reference currents for the resonant controller can be properly computed under generic grid operating conditions from the output signals provided by the DSOGI-FLL.

References

[1] "Towards smart power networks—Lessons learned from European research FP5 projects," European Commission—Office for Official Publications of the European Communities, Luxembourg, Tech. Rep. EUR 21970, 2005.

[2] EWEA (2005), *Large scale integration of wind energy in the European power supply: Analysis, issues and recommendations* [Online]. Available: http://www.ewea.org

[3] F. Blaabjerg, Z. Chen, and S. B. Kjaer, "Power electronics as efficient interface in dispersed power generation systems," *IEEE Trans. Power Electron.*, vol. 19, no. 5, pp. 1184–1194, Sep. 2004.

[4] F. Iov, A. Hansen, P. Sorensen, and N. Cutululis, "Mapping of grid faults and grid codes," Risoe Natl. Lab., Tech. Univ. Denmark, Copenhagen, Tech. Rep., 2007.

[5] E.ON Netz Gmbh (2006, Apr.). *Grid code—high and extra high voltage* [Online]. Available: www.eon-netz.com

[6] *Standard for Interconnecting Distributed Resources With Electric Power Systems*, IEEE Standard 1547, 2003.

[7] UK National grid electricity transmission,"The grid code-revision 21,", Jul. 2007.

[8] I. Erlich, W. Winter, and A. Dittrich, "Advanced grid requirements for the integration of wind turbines into the German transmission system," presented at the IEEE Power Engineering Society General Meeting, Duisburg University, Germany, 2006.

[9] V. M. Moreno, M. Liserre, A. Pigazo, and A. Dell'Aquila, "A comparative analysis of real-time algorithms for power signal decomposition in multiple synchronous reference frames," *IEEE Trans. Power Electron.*, vol. 22, no. 4, pp. 1280–1289, Jul. 2007.

[10] F. Blaabjerg, R. Teodorescu, M. Liserre, and A. V. Timbus, "Overview of control and grid synchronization for distributed power generation systems," *IEEE Trans. Ind. Electron.*, vol. 53, no. 5, pp. 1398–1409, Oct. 2006.

[11] P. Rodriguez, A. Timbus, R. Teodorescu, M. Liserre, and F. Blaabjerg, "Reactive power control for improving wind turbine system behavior under grid faults," *IEEE Trans. Power Electron.*, vol. 24, no. 7, pp. 1798–1801, Jul. 2009.

[12] H. Kim, T. Yu, and S. Choi, "Indirect current control algorithm for utility interactive inverters in distributed generation systems," *IEEE Trans. Power Electron.*, vol. 23, no. 3, pp. 1342–1347, May 2008.

[13] P. S. Flannery and G. Venkataramanan, "A fault tolerant doubly fed induction generator wind turbine using a parallel grid side rectifier and series grid side converter," *IEEE Trans. Power Electron.*, vol. 23, no. 3, pp. 1126–1135, May 2008.

[14] D. Santos-Martin, J. L. Rodriguez-Amenedo, and S. Arnalte, "Direct power control applied to doubly fed induction generator under unbalanced grid voltage conditions," *IEEE Trans. Power Electron.*, vol. 23, no. 5, pp. 2328–2336, Sep. 2008.

[15] C. Meyer, R. W. De Doncker, Y. W. Li, and F. Blaabjerg, "Optimized control strategy for a medium-voltage DVR-theoretical investigations and experimental results," *IEEE Trans. Power Electron.*, vol. 23, no. 6, pp. 2746–2754, Nov. 2008.

[16] M. Tsili and S. Papathanassiou, "A review of grid code technical requirements for wind farms," *IET Renew. Power Generation*, vol. 3, no. 3, pp. 308–332, Sep. 2009.

[17] S. Chung, "A phase tracking system for three phase utility interface inverters," *IEEE Trans. Power Electron.*, vol. 15, no. 3, pp. 431–438, May 2000.

[18] P. Rodriguez, J. Pou, J. Bergas, J. I. Candela, R. P. Burgos, and D. Boroyevich, "Decoupled double synchronous reference frame PLL for power converters control," *IEEE Trans. Power Electron.*, vol. 22, no. 2, pp. 584–592, Mar. 2007.

[19] M. Karimi-Ghartemani and M. R. Iravani, "A method for synchronization of power electronic converters in polluted and variable-frequency environments," *IEEE Trans. Power Syst.*, vol. 19, no. 3, pp. 1263–1270, Aug. 2004.

[20] S. Shinnaka, "A robust single-phase PLL system with stable and fast tracking," *IEEE Trans. Ind. Appl.*, vol. 44, no. 2, pp. 624–633, Mar./Apr. 2008.

[21] M. Ciobotaru, V. G. Agelidis, R. Teodorescu, and F. Blaabjerg, "Accurate and less-disturbing active antiislanding method based on PLL for grid-connected converters," *IEEE Trans. Power Electron.*, vol. 25, no. 6, pp. 1576–1584, Jun. 2010.

[22] M. A. Perez, J. R. Espinoza, L. A. Moran, M. A. Torres, and E. A. Araya, "A robust phase-locked loop algorithm to synchronize static-power converters with polluted AC systems," *IEEE Trans. Power Electron.*, vol. 55, no. 5, pp. 2185–2192, May 2008.

[23] D. Yazdani, M. Mojiri, A. Bakhshai, and G. Joos, "A fast and accurate synchronization technique for extraction of symmetrical components," *IEEE Trans. Power Electron.*, vol. 24, no. 3, pp. 674–684, Mar. 2009.

[24] H. Geng, D. Xu, and B. Wu, "A novel hardware based all digital phase-locked-loop applied to grid-connected power converters," *IEEE Trans. Ind. Electron.*, vol. 58, no. 5, pp. 1737–1745, Jun. 2010.

[25] E. Robles, S. Ceballos, J. Pou, J. Martín, J. Zaragoza, and P. Ibañez, "Variable-frequency grid-sequence detector based on a quasi-ideal low-pass filter stage and a phase-locked loop," *IEEE Trans. Power Electron.*, vol. 25, no. 10, pp. 2552–2563, Oct. 2010.
[26] F. D. Freijedo, J. Doval-Gandoy, O. Lopez, and E. Acha, "A generic open-loop algorithm for three-phase grid voltage/current synchronization with particular reference to phase, frequency, and amplitude estimation," *IEEE Trans. Power Electron.*, vol. 24, no. 1, pp. 94–107, Jan. 2009.
[27] P. Rodriguez, A. Luna, M. Ciobotaru, R. Teodorescu, and F. Blaabjerg, "Advanced grid synchronization system for power converters under unbalanced and distorted operating conditions," in *Proc. 32nd Annu. Conf. IEEE Ind. Electron.*, Nov. 2006, pp. 5173–5178.
[28] P. Rodríguez, A. Luna, I. Candela, R. Mujal, R. Teodorescu, and F. Blaabjerg, "Multiresonant frequency-locked loop for grid synchronization of power converters under distorted grid conditions," *IEEE Trans. Ind. Electron.*, vol. 58, no. 1, pp. 127–138, Jan. 2011.
[29] B. Widrow, J. R. Glover Jr., J. M. McCool, J. Kaunitz, C. S. Williams, R. H. Hearn, J. R. Zeidler, E. Dong Jr., and R. C. Googlin, "Adaptive noise canceling: Principles and Applications," in *Proc. IEEE*, Dec., 1975, vol. 63, no. 12, pp. 1692–1716.
[30] J. R. Glover Jr., "Adaptive noise canceling applied to sinusoidal interferences," *IEEE Trans. Acoust., Speech, Signal Process.*, vol. ASSP-25, no. 6, pp. 484–491, Dec. 1977.
[31] X. Yuan, W. Merk, H. Stemmler, and J. Allmeling, "Stationary frame generalized integrators for current control of active power filters with zero steady-state error for current harmonics of concern under unbalanced and distorted operating conditions," *IEEE Trans. Ind. Appl.*, vol. 38, no. 2, pp. 523–532, Mar./Apr. 2002.
[32] R. Teodorescu, F. Blaabjerg, M. Liserre, and P. C. Loh, "Proportional-resonant controllers and filters for grid-connected voltage-source converters," *IEE Proc. Electric Power Appl.*, vol. 153, no. 5, pp. 750–762, Sep. 2006.
[33] C. Lascu, L. Asiminoaei, I. Boldea, and F. Blaabjerg, "Frequency response analysis of current controllers for selective harmonic compensation in active power filters," *IEEE Trans. Ind. Electron.*, vol. 56, no. 2, pp. 337–347, Feb. 2009.
[34] P. Mattavelli, "A closed-loop selective harmonic compensation for active filters," *IEEE Trans. Ind. Appl.*, vol. 37, no. 1, pp. 81–89, Jan./Feb. 2001.
[35] D. N. Zmood and D. G. Holmes, "Stationary frame current regulation of PWM inverters with zero steady-state error," *IEEE Trans. Power Electron.*, vol. 18, no. 3, pp. 814–822, May 2003.
[36] K. de Brabandere, T. Loix, K. Engelen, B. Bolsens, J. Van den Keybus, J. Driesen, and R. Belmans, "Design and operation of a phase-locked loop with Kalman estimator-based filter for single-phase applications," in *Proc. 32nd Annu. Conf. IEEE Ind. Electron.*, Nov. 2006, pp. 525–530.
[37] M. Mojiri and A. Bakhshai, "An adaptive notch filter for frequency estimation of a periodic signal," *IEEE Trans. Autom. Control*, vol. 49, no. 2, pp. 314–318, Feb. 2004.
[38] M. Mojiri, M. Karimi-Ghartemani, and A. Bakhshai, "Estimation of power system frequency using adaptive notch filter," *IEEE Trans. Instrum. Meas.*, vol. 56, no. 6, pp. 2470–2477, Dec. 2007.
[39] P. Rodriguez, R. Teodorescu, I. Candela, A. V. Timbus, M. Liserre, and F. Blaabjerg, "New positive-sequence voltage detector for grid synchronization of power converters under faulty grid conditions," in *Proc. IEEE Power Electron. Spec. Conf.*, Jun. 2006, pp. 1–7.
[40] M. Ciobotaru, R. Teodorescu, and F. Blaabjerg, "A new single-phase PLL structure based on second order generalized integrator," in *Proc. IEEE Power Electron. Spec. Conf. (PESC'06)*, Jun. 2006, pp. 1–6.
[41] A. Isidori, *Nonlinear Control Systems (Communications and Control Engineering)*, 3rd ed. New York: Springer-Verlag, 1995.
[42] G. F. Franklin, J. D. Powell, and A. Emami-Naeini, *Feedback Control of Dynamic Systems*, 6th ed. Englewood Cliffs, NJ: Prentice-Hall, 2009.
[43] P. Rodriguez, A. Luna, I Candela, R. Teodorescu, and F. Blaabjerg, "Grid synchronization of power converters using multiple second order generalized integrators," in *Proc. 34th Annu. Conf. IEEE Ind. Electron.*, Nov. 2008, pp. 755–760.
[44] W. V. Lyon, *Application of the Method of Symmetrical Components*. New York: McGraw-Hill, 1937.
[45] M. H. J. Bollen, *Understanding Power Quality Problems: Voltage Sags and Interruptions* (Power Engineering Series). Piscataway, NJ: IEEE Press, 2000.

Pedro Rodríguez (S'99–M'04–SM'10) received the B.S. degree from the University of Granada, Granada, Spain, in 1989, and the M.S. and Ph.D. degrees from the Technical University of Catalonia (UPC), Barcelona, Spain, in 1994 and 2004, respectively, all in electrical engineering.

In 1990, he joined as an Assistant Professor in the faculty of UPC where he became an Associate Professor in 1993. He was a Researcher in the Center for Power Electronics Systems, Virginia Polytechnic Institute and State University, Blacksburg, and in the Institute of Energy Technology, Aalborg University, Aalborg, Denmark, in 2005 and 2006, respectively. He is currently the Head of the Research Group on Renewable Electrical Energy Systems, Department of Electrical Engineering, UPC, Barcelona. He has coauthored more than 100 papers in technical journals and conferences. He is the holder of five patents. He has co-organized special sessions in several IEEE conferences on power electronics applied to renewable energies. His research interests include integration of distributed energy systems, power conditioning, and control of power converters.

Dr. Rodriguez is a member of the IEEE Power Electronics, IEEE Industrial Electronics, and IEEE Industry Application Societies and a member of the IEEE-Industrial Electronics Society (IES) Technical Committee on renewable energy systems. He is an Associate Editor of the IEEE TRANSACTION ON POWER ELECTRONICS and the Committee Chair of the IEEE-IES Gold and Student Activities.

Alvaro Luna (S'07–M'10) received the B.Sc., M.Sc., and Ph.D. degrees from the Technical University of Catalonia (UPC), Barcelona, Spain, in 2001, 2005, and 2009, respectively, all in electrical engineering.

He joined as a Faculty Member at UPC in 2005, where he is currently an Assistant Professor. His research interests include wind turbines control, integration of distributed generation, and power conditioning.

Raúl Santiago Muñoz Aguilar received the B.Sc. degree in electrical engineering and the M.Sc. degree in industrial automation from the National University of Colombia, Manizales, Colombia, in 2005 and 2007, respectively. He received the M.Sc. degree in automation and robotics and the Ph.D. degree in advanced automation and robotics from the Technical University of Catalonia (UPC), Barcelona, Spain, both in 2010.

In 2009, he joined as a Faculty Member at UPC, Barcelona, where he is currently an Assistant Professor with the Department of Electrical Engineering.

Ion Etxeberria-Otadui (M'04) received the B.Sc. degree in electronics from the University of Mondragón, Mondragón, Spain, in 1997, and the M.Sc. and Ph.D. degrees from the National Polytechnic Institute of Grenoble, Grenoble, France, in 1999 and 2003, respectively.

From 2003 to 2005, he was the Head of the Power Systems area with the CIDAE Research Center, Mondragón, Spain. Since 2005, he has been a Researcher with the IKERLAN-IK4 Technological Research Center, Mondragón and the Head of the Control Engineering and Power Electronics area, since 2008. His research interests include the application of power electronics devices to distribution networks, electrical traction, and energy-storage applications.

Remus Teodorescu (S'96–A'97–M'99–SM'02) received the Dipl.Ing. degree in electrical engineering from the Polytechnical University of Bucharest, Bucharest, Romania, in 1989, and the Ph.D. degree in power electronics from the University of Galati, Galati, Romania, in 1994.

From 1989 to 1990, he was with Iron and Steel Plant, Galati. He then joined as an Assistant in the Department of Electrical Engineering, University of Galati, Galati, where he has been an Assistant Professor since 1994. In 1996, he was the Head of the Power Electronics Research Group, University of Galati, Galati. In 1998, he joined the Power Electronics and Drives, Department of Energy Technology, Aalborg University, Aalborg East, Denmark, where he is currently a Full Professor. He is the Coordinator for Green Power Research Group and Laboratory with the focus on design and control of grid converters for renewable energy systems. He has published more than 60 papers and one book. He has coauthored more than 100 technical papers 12 of them published in IEEE Transactions, two books, and five patents.

Dr. Teodorescu is an Associate Editor for IEEE POWER ELECTRONICS LETTERS and the chair of the IEEE Danish Industry Application Society (IAS)/Industrial Electronic Society/Power Electronics Society chapter. He is the corecipient of the Technical Committee Prize Paper Awards at IEEE IAS Annual Meeting 1998, and Third-ABB Prize Paper Award at IEEE Optim 2002.

Frede Blaabjerg (S'86–M'88–SM'97–F'03) received the M.Sc.EE. and Ph.D. degrees from Aalborg University, Aalborg East, Denmark, in 1987 and 1995, respectively.

From 1987 to 1988, he was with ABB-Scandia, Randers. From 1988 to 1992, he was a Ph.D. student at Aalborg University, Aalborg East. He became an Assistant Professor, an Associate Professor, and a Full Professor in power electronics and drives, Aalborg University, Aalborg East, in 1992, 1996, and 1998, respectively. In 2000, he was a Visiting Professor at the University of Padova, Padova, Italy as well as a part-time Program Research Leader in wind turbines at Research Center Risoe, Roskilde. From 2006 to 2010, he was the Dean in the Faculty of Engineering, Science and Medicine at Aalborg University, Aalborg East, where he is currently in the Department of Energy Technology. In 2002, he was a Visiting Professor at the Curtin University of Technology, Perth, Australia as well as a Visiting Professor at Zhejiang University, China, in 2009. He has been involved in many research projects with the industry. He is the author or coauthor of more than 600 publications in his research fields including the book "*Control in Power Electronics*." (M. P. Kazmierkowski, R. Krishnan, F. Blaabjerg, Eds. New York: Academic, 2002). His research areas include power electronics, static power converters, ac drives, switched reluctance drives, modeling, characterization of power semiconductor devices and simulation, power quality, wind turbines, custom power systems, and green power inverter.

Dr. Blaabjerg is a member of the European Power Electronics and Drives Association and the IEEE Industry Applications Society Industrial Drives Committee. He is also a member of the Industry Power Converter Committee and the Power Electronics Devices and Components Committee in the IEEE Industry Application Society. He has been an Associate Editor of the IEEE TRANSACTIONS ON INDUSTRY APPLICATIONS, IEEE TRANSACTIONS ON POWER ELECTRONICS, *Journal of Power Electronics*, and the Danish journal Elteknik. Since 2006, he has been an Editor-in-Chief of the IEEE TRANSACTIONS ON POWER ELECTRONICS as well as Distinguished Lecturer for the IEEE Power Electronics Society from 2005 to 2007. He is also a Distinguished Lecturer for the IEEE Industry Applications Society from 2010 to 2011. He received the 1995 Angelos Award for his contribution in modulation technique and control of electric drives and an Annual Teacher Prize at Aalborg University in 1995. In 1998, he received the Outstanding Young Power Electronics Engineer Award from the IEEE Power Electronics Society. He has received nine IEEE Prize Paper Awards during the last ten years (the last in 2008) and another prize paper award at PELINCEC, Poland, in 2005. He received the IEEE Power Electronics Society Distinguished Service Award in 2009 as well as the European Power Electronics and Drives-Power Electronics and Motion Control 2010 Council Award for his contributions in power electronics. In 2002, he received the C.Y. O'Connor Fellowship from Perth, Australia, in 2003, the Statoil Prize for his contributions in Power Electronics, in 2004, the Grundfos Prize in acknowledgement of his international scientific research in power electronics, and finally the Director Ib Henriksen's Research Prize for the acknowledgment of high-level international research in power electronics.